Nuclear Instruments and Methods in Physics Research A 1080 (2025) 170807

Contents lists available at ScienceDirect

Nuclear Inst. and Methods in Physics Research, A

journal homepage: www.elsevier.com/locate/nima

Full Length Article

Simulation of CMOS strip sensors

Naomi Davis [a,*], Jan-Hendrik Arling [a], Marta Baselga [d], Leena Diehl [b,f], Jochen Dingfelder [c], Ingrid-Maria Gregor [a], Marc Hauser [b], Fabian Hügging [c], Karl Jakobs [b], Michael Karagounis [e], Roland Koppenhöfer [b], Kevin Kröninger [d], Fabian Lex [b], Ulrich Parzefall [b], Birkan Sari [d], Niels Sorgenfrei [b,f], Simon Spannagel [a], Dennis Sperlich [b], Anastasiia Velyka [a], Jens Weingarten [d], Yingjie Wei [b], Iveta Zatocilova [b]

[a] Deutsches Elektronen-Synchrotron DESY, Notkestr. 85, 22607 Hamburg, Germany
[b] Physikalisches Institut, University of Freiburg, Hermann-Herder-Straße 3, 79104 Freiburg, Germany
[c] Physikalisches Institut, University of Bonn, Nussallee 12, 53115 Bonn, Germany
[d] Physik E4, TU Dortmund, Otto-Hahn-Strasse 4a, 44227 Dortmund, Germany
[e] Fachhochschule Dortmund, Sonnenstraße 96, 44139 Dortmund, Germany
[f] CERN, Esplanade des Particules 1, 1211 Meyrin, Switzerland

ARTICLE INFO

Keywords:
CMOS
Silicon strip sensors
Test beam
TCAD
Allpix²
Monte Carlo simulation

ABSTRACT

In high-energy physics, there is a need to investigate silicon sensor concepts that offer large-area coverage and cost-efficiency for particle tracking detectors. Sensors based on CMOS imaging technology present a promising alternative silicon sensor concept. As this technology follows an industry process, it can lower sensor production costs and enable fast and large-scale production from various vendors.

The CMOS strips project investigates passive CMOS strip sensors fabricated by LFoundry in a 150 nm technology. The stitching technique was employed to develop two different strip sensor formats. The strip implant layout varies in doping concentration and width, allowing the study of various depletion concepts and electric field configurations.

The performance of the first CMOS strip sensor prototype was evaluated based on several test beam campaigns conducted at the DESY II Test Beam Facility. In order to understand and validate the test beam data results, the detector response was simulated.

This study shows how performance differences of the various strip sensor layouts can be investigated using Monte Carlo methods combined with TCAD Device simulations. In particular, the detector response simulated with Allpix² is presented and compared to test beam data.

1. Introduction

Particle tracking detectors in high-energy physics predominantly use silicon sensors for tracking applications. The ever-increasing sensitive area of these detectors poses a challenge in increasing production volumes and controlling costs to produce silicon sensors. The CMOS strips project studies large-area strip sensors produced in a commercial CMOS process to address this challenge.

The prototype under investigation is a passive CMOS strip sensor fabricated by LFoundry [1] in a 150 nm technology on a 3–5 kΩ cm Float-Zone wafer, with additional backside processing from IZM Berlin. The sensors have a nominal thickness of (150 ± 15) µm and a strip pitch of 75.5 µm. The employed stitching technique creates a short (2.1 cm) and a long (4.1 cm) strip sensor format, as shown in Fig. 1. The n-in-p sensor features three distinct strip implant designs: Regular, Low Dose 30, and Low Dose 55. These differ in both doping concentration and implant widths of 18 µm, 30 µm and 55 µm, respectively. These variations enable the study of different electric field configurations. Representative cross-sections of the Regular and Low Dose 30 implant designs are shown in Fig. 3. Each strip is biased through a polysilicon resistor and read out via an AC-coupled pad, which is wire-bonded to the ALiBaVa readout system [2].

Unirradiated and irradiated samples have been characterised in several test beam campaigns. The sensors show sufficient radiation hardness and no effect of the stitching technique on the sensor performance is observable [3]. The various strip layouts, however, show distinct performance differences in test beam data, which are studied

* Corresponding author.
E-mail address: naomi.davis@desy.de (N. Davis).

https://doi.org/10.1016/j.nima.2025.170807
Received 16 April 2025; Received in revised form 17 June 2025; Accepted 25 June 2025
Available online 4 July 2025

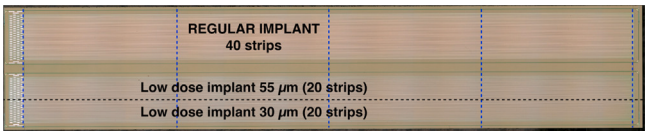

Fig. 1. Microscopic view of a passive CMOS strip sensor with a length of 4.1 cm, showing two active areas with variation in the strip implant design. Blue dashed lines mark stitching regions along the sensor. [4].

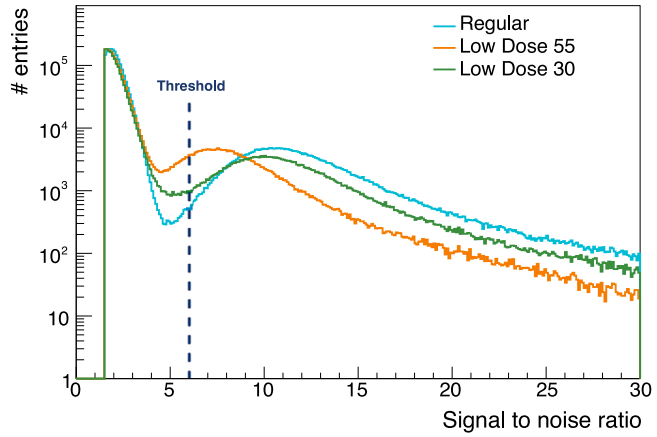

Fig. 2. Seed strip SNR distribution for test beam data of a short strip sensor sample. The SNR distribution comprises a partial Gaussian noise distribution and a Landau-shaped signal distribution. The dashed line indicates the final threshold cut in the clustering procedure.

with a dedicated software tool for sensor simulations and described in the following.

2. Test beam measurement

2.1. Experimental setup

The prototype performance of an unirradiated short sample was measured at the DESY II Test Beam Facility [5]. The test beam setup includes the ADENIUM pixel telescope [6] as a reference for particle tracking with the prototype placed in the center. A 4.2 GeV electron beam is directed onto the telescope planes, and two scintillators with PMTs trigger the setup. A detailed description of the experimental setup is provided in [7].

2.2. Clustering

The test beam data is read, reconstructed and analysed with the Corryvreckan framework [8]. The initial stage of test beam data reconstruction is to group adjacent strips that registered a hit into clusters. The clustering algorithm used in this analysis groups adjacent strips based on their individual signal-to-noise ratio (SNR). Fig. 2 shows the seed strip SNR distribution for all three strip implant layouts. The left peak partially indicates the Gaussian noise distribution, while the right peak is the Landau distribution of the signal. A cut in the SNR distribution, as depicted in Fig. 2, defines the clustering threshold.

To build a cluster, the algorithm selects the strip with the highest SNR in an event. If the corresponding SNR is above the threshold, the strip is defined as a seed strip and neighbouring strips are added iteratively if their signal level is above the set threshold. Fig. 2 indicates that the SNR distributions are shifted to smaller values for the large collection electrode designs. This behaviour is also reflected in the total efficiency as a function of the threshold as previously shown [3]. To understand these performance differences, the different sensor layouts are investigated in depth with sensor simulations.

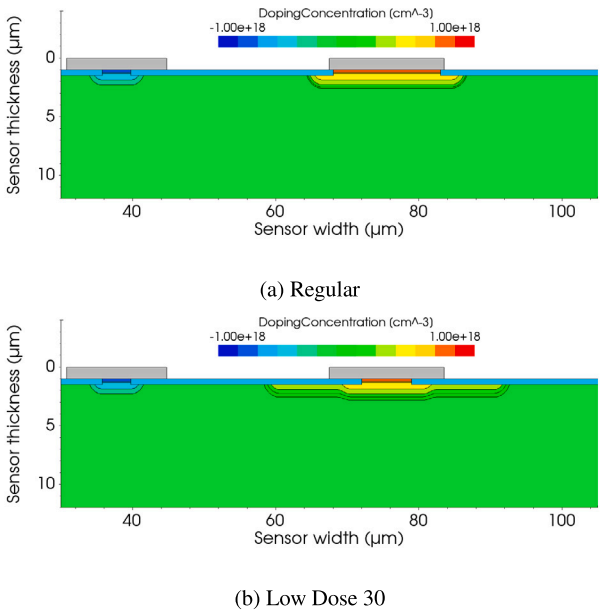

Fig. 3. Section of the simulated 2D TCAD strip sensor model. It shows one n-type strip implant (red and yellow) adjacent to a p-stop implant (blue). The implants are covered by a silicon oxide layer (turquoise) and metal contacts (grey). The sensor bulk (green) is not shown in full depth.

3. Simulation method

3.1. TCAD simulation

The first step in simulating the sensor response is to build a 2D model of the strip sensor. The model is created with electrostatic Technology Computer-Aided Design (TCAD) simulations provided by Synopsys Sentaurus [9], as in previous studies presented in [3]. The model is based on fundamental sensor characteristics, such as the strip pitch, the nominal thickness, the wafer resistivity and the implant width for the Regular and Low Dose designs.

Fig. 3 shows the 2D model of the sensor structure for the Regular and LD30 designs with the colour scale representing the doping concentration of the p- and n-doped regions. Both designs have a constant p-doping concentration in the sensor bulk. The strip implant is located in the centre of Figs. 3(a) and 3(b). In Fig. 3(a) for the Regular design, the strip implant consists of a highly doped n^+ layer with a lower doped, 18 μm wide n-implant below.

For the Low Dose design depicted in Fig. 3(b), the strip implant has a reduced width of 10 μm for the highly doped n^+ layer and the lesser doped n-implant layer is extended by low-doped n-implants on each side with a total width of 30 μm. The p-stop implants on either side in both models electrically isolate the strip implants. All implants are located partially beneath a silicon oxide layer and are contacted by metal layers. The full sensor model has a thickness of 150 μm, corresponding to the nominal sensor thickness. Another metal contact is located on the sensor backside, which is not depicted in Fig. 3.

The next simulation step is to apply a bias voltage to the model. Fig. 4 shows the electric field strength, including the equipotential lines, simulated for the Regular and Low Dose 30 designs at a bias voltage of −100 V. The complete sensor thickness runs along the y-axis, and the sensor width along the x-axis. At the applied bias voltage of −100 V, the sensor bulk is fully depleted, as indicated by the white line marking the extent of the depletion region. The strip implant is located in the middle of each plot, and the p-stop implants are shown on the edges. The electrically isolating effect of the p-stop implants is clearly visible. The field strength is highest around the implant region for both designs and slightly varies in shape for the different designs.

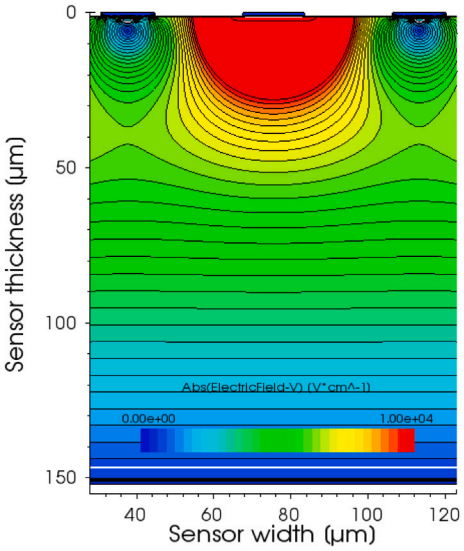

(a) Regular

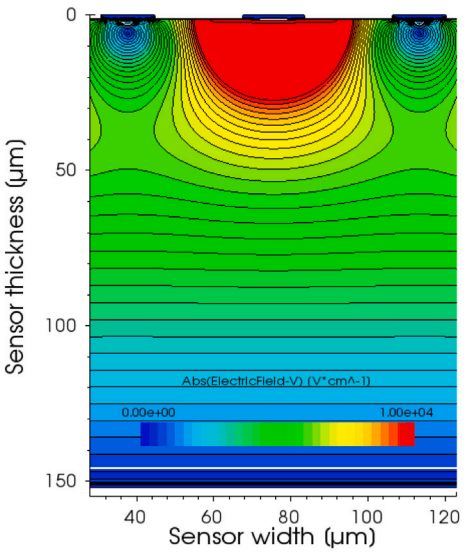

(b) Low Dose 30

Fig. 4. Electric field strength in the sensor bulk as simulated with TCAD at a bias voltage of −100 V. The figure shows a single strip implant in the center surrounded by two p-stop implants. Metallic contacts cover the top of the implants. The colour scale indicates the absolute electric field strength.

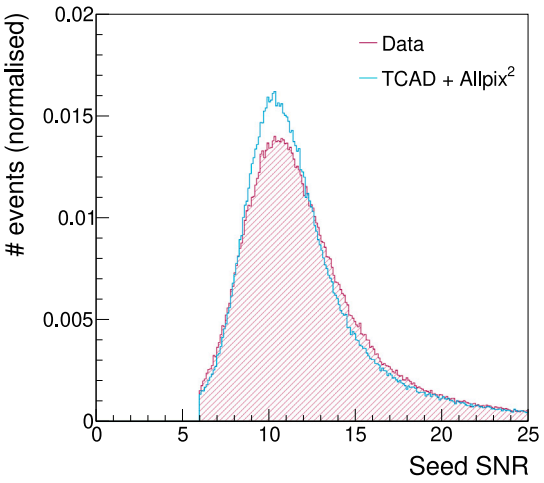

(a) Regular

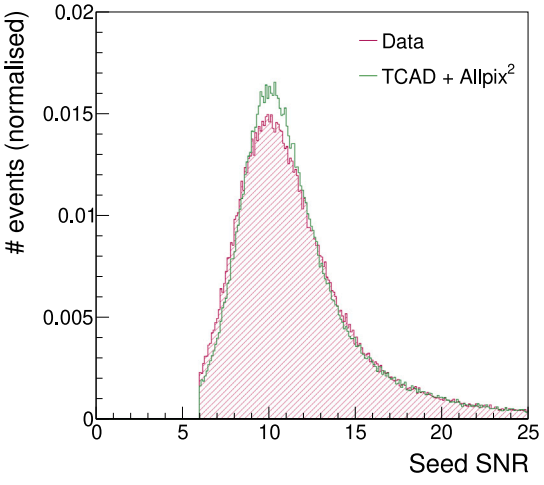

(b) Low Dose 30

Fig. 5. The seed strip SNR distribution for data and simulation of a short strip sample. The distribution is cut at a SNR of six as the clustering threshold.

To relate the different electric field configurations to the sensor performance, the sensor response to an impinging electron beam is simulated using the Allpix^2 framework.

3.2. *Allpix*^{2}

The Allpix^2 framework [10] allows running high-statistics Monte Carlo simulations of the sensor response. The electric field and doping concentrations simulated with TCAD are imported into the Allpix^2 framework. The sensor response is simulated by directing an electron beam of 4.2 GeV onto a strip detector model comprised of the sensor designs described above. The detector model consists of a 1 × 20 strip matrix for the Low Dose 30 design and a 1 × 40 strip matrix for the Regular design, according to the number of strips in each active region, as denoted in Fig. 1.

The Allpix^2 sensor simulation includes several simulation stages. In the first stage, after the charge deposition resulting from the interaction of the incident electrons with the sensor material, the generated charge is propagated by drift and diffusion towards the collection electrodes.

After the charge carrier propagation, the capacitive coupling to the strip sensor front end is simulated using the `[CapacitiveTransfer]` module in Allpix^2. For this, the coupling capacitance to the front end, the bulk capacitance, and the interstrip capacitance between neighbouring strips are considered. Based on these capacitances, the charge fractions on the leading strip, which registered a hit, and on the adjacent strips are calculated. These charge fractions are handed to the `[CapacitiveTransfer]` module as a 3 × 1 coupling matrix. Accordingly, propagated charges are copied on adjacent strips or reduced on the leading strip in the simulation.

In the following digitisation stage, noise is added to the sensor response. The noise level is estimated from data to be around 1000–1200 e^-, depending on the sensor design. The noise is added to

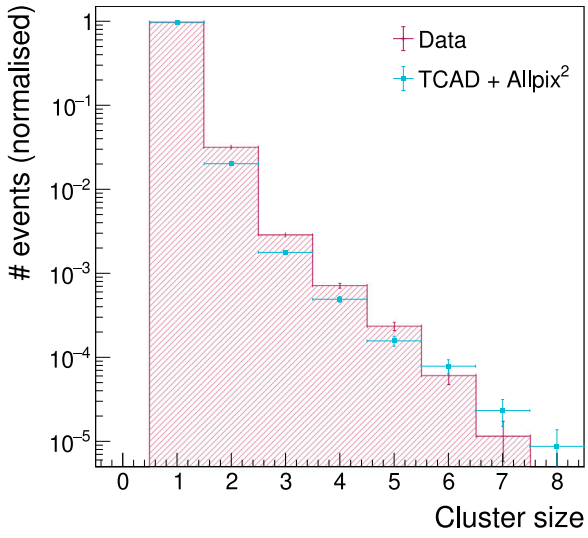

(a) Regular

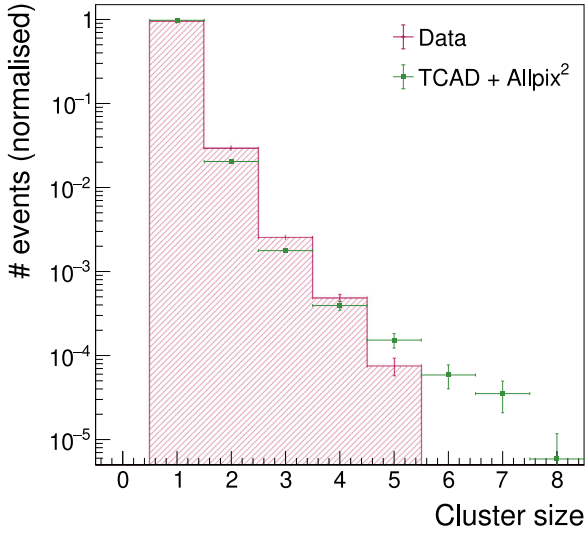

(b) Low Dose 30

Fig. 6. The cluster size distribution for data and simulation of a short strip sample. The clustering threshold is at a SNR of six.

every strip channel, independent of a charge deposition on the strip. In this way, the permanent noise level present on every strip readout channel is recreated in the simulation.

4. Results

The simulation results at the digitisation stage of the Allpix² framework can be analysed using the Corryvreckan framework. To compare the simulation results to test beam data, the simulation output is reconstructed with the same clustering algorithm applied to the data and described in Section 2.

In data and simulation, a clustering threshold of a SNR of six is applied to exclude the main part of the noise distribution from the signal, as illustrated in Fig. 2.

4.1. Signal-to-noise ratio

As an example, Fig. 5 shows the seed strip SNR distribution as reconstructed from test beam data and the combination of TCAD and Allpix² simulation for the Regular and Low Dose 30 designs. Simulation and data show a good agreement for both designs, and the results are comparable.

However, the simulation shows deviations at the flanks of the distribution. The data distribution appears to be smeared more than the simulated distribution results. This deviation could be related to the readout chip gain dispersion in data that is not considered to the same extent in the simulation and will be examined further.

4.2. Cluster size

Fig. 6 shows the cluster size distribution of the Regular and Low Dose 30 designs for data and simulation. For both designs, the most significant fraction of clusters in data are one and two-strip clusters, which is reflected by the simulation results showing a general agreement. For cluster sizes $>$ 4, the statistics decrease significantly in data as well as in the simulation, and the deviation between data and simulation increases. Especially for the LD30 design, the simulation cannot describe the data well. The behaviour at large cluster sizes is still under investigation, as is the completion of the data and simulation comparison for the LD55 design.

5. Conclusion

The test beam data shows performance differences in the Regular and Low Dose strip implant designs. These performance differences can be studied by simulating the sensor response in the Allpix² framework, with the sensor doping concentrations and electric field provided by electrostatic TCAD simulations. The simulation output, analysed with Corryvreckan, shows good agreement with test beam data for single-strip clusters. However, deviations remain for wider clusters, indicating the need for further investigation.

A short-term goal is to compare additional performance indicators, such as spatial resolution and efficiency. Furthermore, the simulation setup will be optimised for parameters like the readout chip gain.

In the long term, the CMOS strip project strives for a monolithic chip design by adding an active front end to the strip sensors.

Declaration of competing interest

The authors declare that they have no known competing financial interests or personal relationships that could have appeared to influence the work reported in this paper.

Acknowledgements

The measurements leading to these results have been performed at the Test Beam Facility at DESY Hamburg (Germany), a member of the Helmholtz Association (HGF).

References

[1] LFoundry, LFoundry S.r.l. Landshut, Ludwig-Erhard-Strasse 6A, 84034 Landshut, Germany, 2021, URL http://www.lfoundry.com/en/.

[2] R. Marco-Hernandez, A portable readout system for microstrip silicon sensors (ALIBAVA), IEEE Trans. Nucl. Sci. 56 (3) (2009) 1642–1649, http://dx.doi.org/10.1109/TNS.2009.2017261.

[3] I. Zatocilova, J.-H. Arling, M. Baselga, N. Davis, L. Diehl, J. Dingfelder, I.-M. Gregor, M. Hauser, T. Hemperek, F. Hügging, K. Jakobs, M. Karagounis, R. Koppenhöfer, K. Kröninger, F. Lex, U. Parzefall, A. Rodriguez, B. Sari, N. Sorgenfrei, S. Spannagel, D. Sperlich, T. Wang, J. Weingarten, Characterisation, simulation and test beam data analysis of stitched passive CMOS strip sensors, Nucl. Instrum. Methods Phys. Res. Sect. A: Accel. Spectrometers Detect. Assoc. Equip. 1061 (2024) 169132, http://dx.doi.org/10.1016/j.nima.2024.169132.

[4] L. Diehl, M. Baselga, I.M. Gregor, M. Hauser, T. Hemperek, J.C. Hönig, K. Jakobs, S. Mägdefessel, U. Parzefall, A. Rodriguez, S. Sharma, D. Sperlich, L. Wiik-Fuchs, T. Wang, Characterization of passive CMOS strip sensors, Nucl. Instrum. Methods Phys. Res. Sect. A: Accel. Spectrometers Detect. Assoc. Equip. 1033 (2022) 166671, http://dx.doi.org/10.1016/j.nima.2022.166671.

[5] R. Diener, J. Dreyling-Eschweiler, H. Ehrlichmann, I. Gregor, U. Kötz, U. Krämer, N. Meyners, N. Potylitsina-Kube, A. Schütz, P. Schütze, M. Stanitzki, The DESY II test beam facility, Nucl. Instrum. Methods Phys. Res. Sect. A: Accel. Spectrometers Detect. Assoc. Equip. 922 (2019) 265–286, http://dx.doi.org/10.1016/j.nima.2018.11.133.

[6] Y. Liu, C. Feng, I.-M. Gregor, A. Herkert, L. Huth, M. Stanitzki, Y. Teng, C. Yang, ADENIUM — A demonstrator for a next-generation beam telescope at DESY, J. Instrum. 18 (06) (2023) P06025, http://dx.doi.org/10.1088/1748-0221/18/06/P06025.

[7] N. Davis, J.-H. Arling, M. Baselga, L. Diehl, J. Dingfelder, I.-M. Gregor, M. Hauser, F. Hügging, T. Hemperek, K. Jakobs, M. Karagounis, R. Koppenhöfer, K. Kröninger, F. Lex, U. Parzefall, A. Rodriguez, B. Sari, N. Sorgenfrei, S. Spannagel, D. Sperlich, T. Wang, J. Weingarten, I. Zatocilova, Characterisation and simulation of stitched CMOS strip sensors, Nucl. Instrum. Methods Phys. Res. Sect. A: Accel. Spectrometers Detect. Assoc. Equip. 1064 (2024) 169407, http://dx.doi.org/10.1016/j.nima.2024.169407.

[8] D. Dannheim, K. Dort, L. Huth, D. Hynds, I. Kremastiotis, J. Kröger, M. Munker, F. Pitters, P. Schütze, S. Spannagel, T. Vanat, M. Williams, Corryvreckan: a modular 4D track reconstruction and analysis software for test beam data, J. Instrum. 16 (03) (2021) P03008, http://dx.doi.org/10.1088/1748-0221/16/03/P03008.

[9] Synopsys TCAD, 2025, URL https://www.synopsys.com/manufacturing/tcad.html.

[10] S. Spannagel, K. Wolters, D. Hynds, N. Alipour Tehrani, M. Benoit, D. Dannheim, N. Gauvin, A. Nürnberg, P. Schütze, M. Vicente, Allpix2: A modular simulation framework for silicon detectors, Nucl. Instrum. Methods Phys. Res. Sect. A: Accel. Spectrometers Detect. Assoc. Equip. 901 (2018) 164–172, http://dx.doi.org/10.1016/j.nima.2018.06.020.